Available online at www.sciencedirect.com
SCIENCE DIRECT®
International Journal of Thermal Sciences 42 (2003) 1003–1012
International Journal of Thermal Sciences
www.elsevier.com/locate/ijts

Laminar free convection and entropy generation inside an inclined wavy enclosure

Shohel Mahmud [a,*], A.K.M. Sadrul Islam [b]

[a] *Department of Mechanical Engineering, University of Waterloo, 200 University Avenue West, Waterloo, ON, Canada N2L3G1*
[b] *Department of Mechanical Engineering, Bangladesh University of Engineering and Technology (BUET), Dhaka 1000, Bangladesh*

Received 19 August 2002; accepted 5 February 2003

Abstract

We investigate numerically the heat transfer and fluid flow characteristics inside a wavy walled enclosure. Second law of thermodynamics is also applied to predict the nature of irreversibility in terms of entropy generation. Finite-volume method is used to discretize the governing differential equations with non-staggered variable arrangement. SIP (strongly implicit procedure) solver solves the linear equation systems with full multigrid (FMG) acceleration. Simulation was carried out for a range of wave ratio (defined by amplitude/average width) $\lambda = 0.0$–0.4, aspect ratio (defined by height/average width) $A = 1.0$–2.0, Rayleigh number $Ra = 10^0$–10^7 for a fluid having Prandtl number equal to 0.7. The angle of inclination (θ) is varied from 0° to 360° with 15° interval. Streamlines and isothermal lines represent the corresponding flow and thermal fields. Local and global Nusselt number distributions express the rate of heat transfer. Contour of Bejan number is plotted. Volume averaged entropy generation rate is also presented.

Keywords: Entropy generation; Finite-volume method; Irreversibility; Laminar flow; Natural convection; Wavy wall

1. Introduction

Geometrical complexity restricts wide-variety analyses of heat transfer and fluid flow problems inside wavy-walled enclosures. Literatures related to this topic are not as rich as enclosures with flat walls. Whatever the shape of the wall, flow and heat transfer problems inside enclosures have numerous engineering applications like solar-collectors, double-wall insulation, electric machinery, cooling system of electronic devices, natural circulation in the atmosphere, the molten core of the Earth, etc. Always there is a possibility of complex interaction between finite fluid content inside the enclosure with the enclosure walls. This complexity increases when the wall becomes wavy or with the change of orientation of the enclosure. Addition of irreversibility analysis makes situation more complicated.

Adjlout et al. [1] reported natural convection in an inclined cavity with hot wavy wall and cold flat wall. One of their interesting findings was the decrease of average heat transfer with the surface waviness when compared with flat wall cavity. For both (hot and cold) wavy walls, Mahmud et al. [2] recently presented the flow and heat transfer characteristics inside a vertical wavy walled enclosure. They also reported the decrease of average heat transfer with the increase of surface waviness. Hadjadj and Kyal [3] numerically investigated the effect of sinusoidal protuberances on heat transfer and fluid flow inside an annular space using a non-orthogonal coordinate transformation. They reported that both local and average heat transfer increase with the increase of protuberances amplitude and Rayleigh number and decreasing Prandtl number. Kumar [4] presented the parametric results of flow and thermal field inside a vertical wavy enclosure with pours media. He concluded that the surface temperature was very sensitive to the drifts in the surface undulations, phase of the wavy surface and number of the wave. Yao [5] presented the near wall characteristics of flow and thermal field of a vertical wavy wall. Saidi et al. [6] presented numerical and experimental results of flow over and heat transfer from a sinusoidal cavity. They reported that the total heat exchange between the wavy wall of the cavity and flowing fluid was reduced by the presence of vortex. Vortex plays the role of a thermal screen, which creates

* Corresponding author.
E-mail addresses: smahmud@engmail.uwaterloo.ca (S. Mahmud), sadrul@me.buet.ac.bd (A.K.M.S. Islam).

1290-0729/$ – see front matter
doi:10.1016/S1290-0729(03)00076-0

Nomenclature

a	amplitude of the wave	m	
A	aspect ratio, $= H/W$		
Be	Bejan number (see Eq. (11))		
Br	Brinkman number, $= Ec \times Pr$		
C_P	specific heat	$kJ{\cdot}kg^{-1}{\cdot}K^{-1}$	
Ec	Eckert number, $= V_0^2/(C_p \Delta T)$		
FFI	fluid friction irreversibility		
HTI	heat transfer irreversibility		
$\mathbf{g}$	gravity vector	$m{\cdot}sec^{-1}$	
H	height of the cavity	m	
h	heat transfer coefficient	$W{\cdot}m^{-2}{\cdot}K^{-1}$	
k	thermal conductivity	$W{\cdot}m^{-1}{\cdot}K^{-1}$	
N_S	entropy generation number, $= \dot{S}'''_{\text{gen}}/\dot{S}'''_c$		
Nu	Nusselt number, $= h \cdot W/k$		
Pr	Prandtl number, $= \nu/\alpha$		
p	pressure	Pa	
P	dimensionless pressure, $= p/(\rho V_0^2)$		
Ra	Rayleigh number, $= Gr \times Pr$		
$\dot{S}'''_{\text{gen}}$	entropy generation rate	$W{\cdot}m^{-3}{\cdot}K^{-1}$	
$\dot{S}'''_c$	characteristic entropy transfer rate	$W{\cdot}m^{-3}{\cdot}K^{-1}$	
T	temperature	°C	
T_0	reference temperature	°C	
u	velocity component in x-direction	$m{\cdot}sec^{-1}$	
U	dimensionless velocity component, $= u/V_0$		
v	velocity component in y-direction	$m{\cdot}sec^{-1}$	
V	dimensionless velocity component, $= v/V_0$		
W	average width of the cavity	m	
x	horizontal coordinate		
X	dimensionless horizontal coordinate		
y	vertical coordinate		
Y	dimensionless vertical coordinate		

Greek symbols

α	thermal diffusivity	$m^2{\cdot}sec^{-1}$	
β	thermal expansion coefficient	K^{-1}	
Δ	difference between tow values		
λ	surface waviness, $= a/W$		
ρ	density of the fluid	$kg{\cdot}m^{-3}$	
ν	kinematic viscosity	$m^2{\cdot}sec^{-1}$	
Ω	dimensionless temperature difference, $= \Delta T/T_0$		
Θ	dimensionless temperature		

Subscripts

av	average value
L	local value
w	value at the wall

a large region of uniform temperature in the bottom of the cavity. Asako and Faghri [7] and Mahmud et al. [8] gave a Finite-volume prediction of heat transfer and fluid flow characteristics inside a wavy walled duct and tube respectively. Lage and Bejan [9] documented heat transfer results near a periodically (timewise and spatial) stretching wall. Hossain and Rees [10], Moulic and Yao [11] and Rees and Pop [12] presented similarity solutions for natural convection flow near wavy surface at different boundary conditions. Hamady et al. [13], Ozoe et al. [14], Elsherbiny [15], Sundstrom and Kimura [16] and Aydin [17] presented results of heat transfer characteristics inside rectangular enclosure at different aspect ratios and orientations without surface waviness.

The problems studied in the foregoing references are restricted, in the thermodynamic point of view, to only the first law (of thermodynamics) analysis. The contemporary trend in the field of heat transfer and thermal design is the second law (of thermodynamics) analysis and its design-related concept of entropy generation and its minimization (Bejan [18]). This new trend is important and, at the same time, necessary, if the heat transfer community is to contribute to a viable engineering solution to the energy problems. Entropy generation is associated with thermodynamic irreversibility, which is present in all types of heat transfer processes. Different sources of irreversibility are responsible for heat transfer's generation of entropy like heat transfer across finite temperature gradient, characteristics of convective heat transfer, viscous effects, etc. Bejan [18] focused on the different reasons behind entropy generation in applied thermal engineering. The generation of entropy destroys the available work of a system. Therefore, it makes good engineering sense to focus on the irreversibility of heat transfer and fluid flow processes, and try to understand the function of the entropy generation mechanism(s). For a comprehensive reference, see Baytas [19], Bejan [20] and Mahmud and Fraser [21].

This paper presents characteristics of flow, heat transfer and entropy generation inside an inclined enclosure bounded by two isothermal wavy walls and two adiabatic straight walls at different Rayleigh numbers and orientations for some selected values of surface waviness and aspect ratio.

2. Mathematical modeling

Considering two-dimensional laminar natural convection of an incompressible Newtonian fluid in a cavity with two wavy walls and two flat walls. The corresponding height, average width, and the amplitude of the wavy wall are H, W, and a, respectively. Modeling the flow as 'Boussinesq-incompressible' to take into account the coupling between the energy and momentum equations, we regard the density ρ as constant everywhere except in the buoyancy term of momentum equations (Eqs. (2) and (3)). Correspondingly, the non-dimensional equations governing the conservation

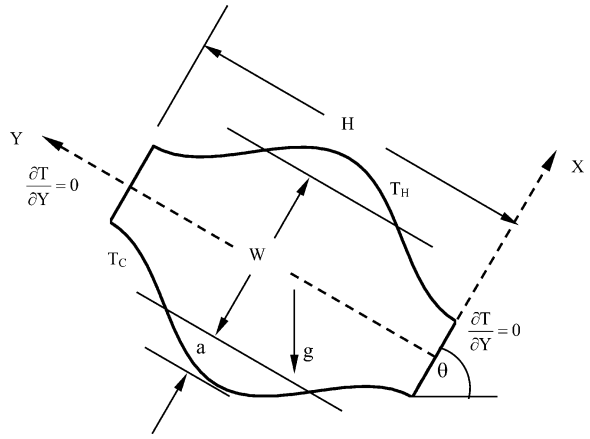

Fig. 1. Schematic diagram of the problem under consideration.

of mass, momentum, and energy in the cavity of Fig. 1 are as follows

$$\frac{\partial U}{\partial X}+\frac{\partial V}{\partial Y}=0 \tag{1}$$

$$\frac{\partial U}{\partial \tau}+U\frac{\partial U}{\partial X}+V\frac{\partial U}{\partial Y} =-\frac{\partial P}{\partial X}+\Theta\sin\theta+\sqrt{\frac{Pr}{Ra}}\left(\frac{\partial^2 U}{\partial X^2}+\frac{\partial^2 U}{\partial Y^2}\right) \tag{2}$$

$$\frac{\partial V}{\partial \tau}+U\frac{\partial V}{\partial X}+V\frac{\partial V}{\partial Y} =-\frac{\partial P}{\partial Y}+\Theta\cos\theta+\sqrt{\frac{Pr}{Ra}}\left(\frac{\partial^2 V}{\partial X^2}+\frac{\partial^2 V}{\partial Y^2}\right) \tag{3}$$

$$\frac{\partial \Theta}{\partial \tau}+U\frac{\partial \Theta}{\partial X}+V\frac{\partial \Theta}{\partial Y} =\frac{1}{\sqrt{Pr\,Ra}}\left(\frac{\partial^2 \Theta}{\partial X^2}+\frac{\partial^2 \Theta}{\partial Y^2}\right) \tag{4}$$

Eqs. (1)–(4) are put into their dimensionless forms by scaling different lengths with average width W, velocity components with reference velocity, V_0, which is equal to $(g\beta\Delta T W)^{1/2}$, pressure with ρV_0^2, time with W/V_0. The dimensionless temperature can be defined as $\Theta=(T-T_C)/\Delta T$ where ΔT is equal to (T_H-T_C). According to Bejan [18], the entropy generation equation in dimensionless form

$$N_S=\left[\left(\frac{\partial \Theta}{\partial X}\right)^2+\left(\frac{\partial \Theta}{\partial Y}\right)^2\right] +\frac{Br}{\Omega}\left[2\left\{\left(\frac{\partial U}{\partial X}\right)^2+\left(\frac{\partial V}{\partial Y}\right)^2\right\}+\left(\frac{\partial U}{\partial Y}+\frac{\partial V}{\partial Y}\right)^2\right] \tag{5}$$

where entropy generation number N_S is the ratio of entropy generation rate $\dot{S}'''_{gen}$ and characteristic entropy transfer rate, $\dot{S}'''_c$, which is equal to $k\Delta T^2/(T_0^2W^2)$. Br and Ω are the Brinkman number and dimensionless temperature difference, respectively. The ratio of Br and Ω is generally named as group parameter. T_0 is a reference temperature and for the present investigation, T_0 is put equal to T_C.

2.1. Boundary and initial conditions

Fig. 1 shows the geometry under consideration in the present investigation with different boundary conditions and axis system. Two straight walls of the cavity are kept adiabatic. The wavy walls are isothermal and kept at different temperatures. The surface wave shape of the wavy walls follows the equations given in Eqs. (6c) and (6d). The hot and cold wall temperatures are T_H and T_C. The gravity acceleration **g** is acted downwards. No slip boundary condition is applied for velocity components at both isothermal and adiabatic walls. Boundary conditions can be summarized by the following equations:

$$\tau\geqslant 0,\qquad Y=0,\qquad -\left(\frac{1}{2}-\lambda\right)\leqslant X\leqslant\left(\frac{1}{2}-\lambda\right)$$
$$U=V=0,\qquad \frac{\partial\Theta}{\partial Y}=0 \tag{6a}$$

$$\tau\geqslant 0,\qquad Y=A,\qquad -\left(\frac{1}{2}-\lambda\right)\leqslant X\leqslant\left(\frac{1}{2}-\lambda\right)$$
$$U=V=0,\qquad \frac{\partial\Theta}{\partial Y}=0 \tag{6b}$$

$$\tau\geqslant 0,\qquad 0\leqslant Y\leqslant A$$
$$X=\left(\frac{1}{2}-\lambda\right)+\lambda\left[1-\sin\frac{\pi}{2}\left(1+\frac{4Y}{A}\right)\right]$$
$$U=V=0,\qquad \Theta=1 \tag{6c}$$

$$\tau\geqslant 0,\qquad 0\leqslant Y\leqslant A$$
$$X=-\left(\frac{1}{2}-\lambda\right)-\lambda\left[1-\sin\frac{\pi}{2}\left(1+\frac{4Y}{A}\right)\right]$$
$$U=V=0,\qquad \Theta=0 \tag{6d}$$

As the initial condition, a motionless state and uniform temperature are taken:

At $\tau=0,\quad 0<Y<A$

and

$$-\left(\frac{1}{2}-\lambda\right)-\lambda\left[1-\sin\frac{\pi}{2}\left(1+\frac{4Y}{A}\right)\right]<X <\left(\frac{1}{2}-\lambda\right)+\lambda\left[1-\sin\frac{\pi}{2}\left(1+\frac{4Y}{A}\right)\right]$$
$$U=V=\Theta=0 \tag{7}$$

2.2. Solution methodology

To conduct a numerical analysis for the thermofluid dynamics fields, we used the technique similar as Hortmann et al. [22] based on the finite-volume method as described in Ferziger and Peric [23]. The solution domain is first subdivided into finite number of control volumes (CV). Body fitted, non-orthogonal grids are oriented in such a way that the number of CV is higher near the walls. All variables are calculated at the center of each CV (non-staggered scheme). SIMPLE algorithm is used.

First the momentum equations (Eq. (2) and Eq. (3)) are discretized and linearized. Convective fluxes are approximated using UDS scheme with linear deferred correction (Ferziger and Peric [23]) which is second order accurate. CDS scheme approximated diffusive fluxes. Discretized momentum equations lead to an algebraic equation systems for velocity components U and V where pressure, temperature, fluid properties are taken from the previous iteration except the first iteration where initial conditions are applied. These linear equation systems are solved iteratively (inner iteration) to obtain an improved estimate of velocity. The improved velocity field is then used to estimate new mass fluxes, which satisfy the continuity equation. Pressure-correction equation is then solved using the same linear equation solver and to the same tolerance. Energy equation is then solved in the same manner to obtain better estimate of new solution. This completes one outer iteration and is repeated until residual level is less than or equal to 10^{-5} at a particular time step. Then the above procedure is repeated for a new time step. For time marching, we selected '*Three Time Level Method*' which is a fully implicit scheme of second order accurate. For details of this method, see Ferziger and Peric [23]. In this study the SIP-solver based on lower-upper decomposition (ILU) is used to solve the linear equation systems. To avoid divergence, underrelaxation parameter 0.7 is used for velocity, 0.2 for pressure and 0.9 for temperature. Once steady-state converged solution is attained, entropy generation number is calculated using the converged value of U, V, Θ from Eq. (5).

2.3. Accuracy assessment

Accuracy of the numerical method is tested with three combinations (16×32, 32×64, and 64×128) of grid-size. Profiles for V-velocity are plotted at the mid-height ($Y = A/2$) of the cavity (Fig. 2(a)) for $Ra = 10^4$, $\lambda = 0.25$, $\theta = 0^0$, and $A = 2.0$. Velocity profile for coarse grid (16×32) shows some deviation with medium coarse (32×64) and fine (64×128) grids. Variation between the profiles of medium coarse and fine grids is very small. Maximum percentage deviation of the magnitude of velocity between coarse (16×32) and fine grid (64×128) solution is 4% and medium-coarse (32×64) and fine-grid (64×128) is 1.5%, respectively. Throughout this study the results are presented for 64×128 CVs'.

Predicted results of average Nusselt number for a square cavity ($A = 1$, $\lambda = 0$, $\theta = 0^0$) with the same boundary conditions are compared with the benchmark solution of Hortmann et al. [22] and with the experimental data of Hamady et al. [13] and Markatos and Pericleous [24]. Fig. 2(b) shows this comparison. Predicted results show a very good agreement with the reference benchmark solution and experimental works.

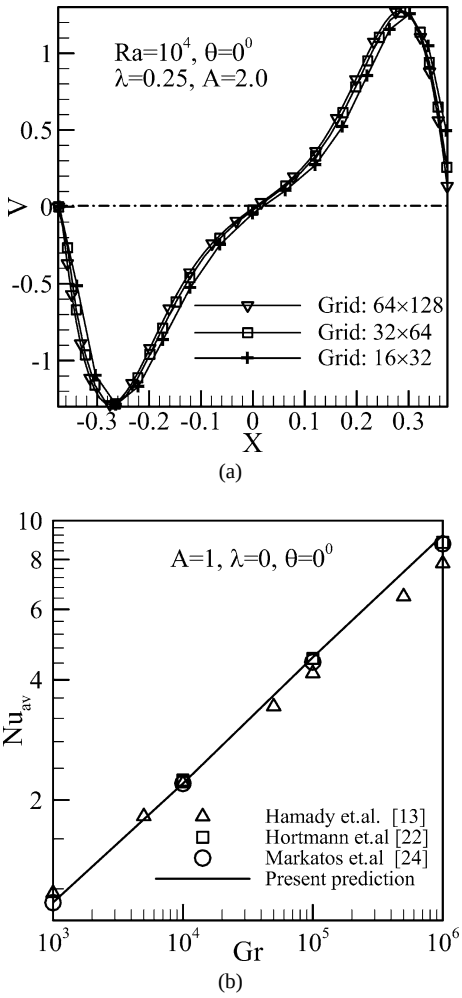

Fig. 2. (a) Velocity profiles at $Y = 0.5$ for three different grid sizes. (b) Comparison of present prediction with benchmark solutions and experimental results.

3. Results and discussions

3.1. Flow and thermal field

The patterns of the flow and thermal fields are presented in Fig. 3(a)–(h) in terms of streamlines and isothermal lines for a constant Rayleigh number ($Ra = 10^5$) keeping wall waviness ($\lambda = 0.25$) and aspect ratio ($A = 2.0$) constant. For a particular angle of orientation ($\theta = 0°$), effect of Rayleigh number on the flow and thermal fields are available in Mahmud et al. [2]. Eight different angular positions (θ) are selected (see Fig. 3(a)–(h)). For the convenience of presentation, magnitudes of the streamfunction are made dimensionless by dividing individual values with the maximum value of the streamfunction ($\psi_{\max}$) for each case. Values of the streamfunction then range between 0 to 1. Maximum value of the streamfunction for each angular orientation is given in Fig. 3(a)–(h). Fig. 3(a) shows the flow and thermal field for $\theta = 0°$. Hot fluid moves up along the hot wall, turns to the left near the top adiabatic wall and then

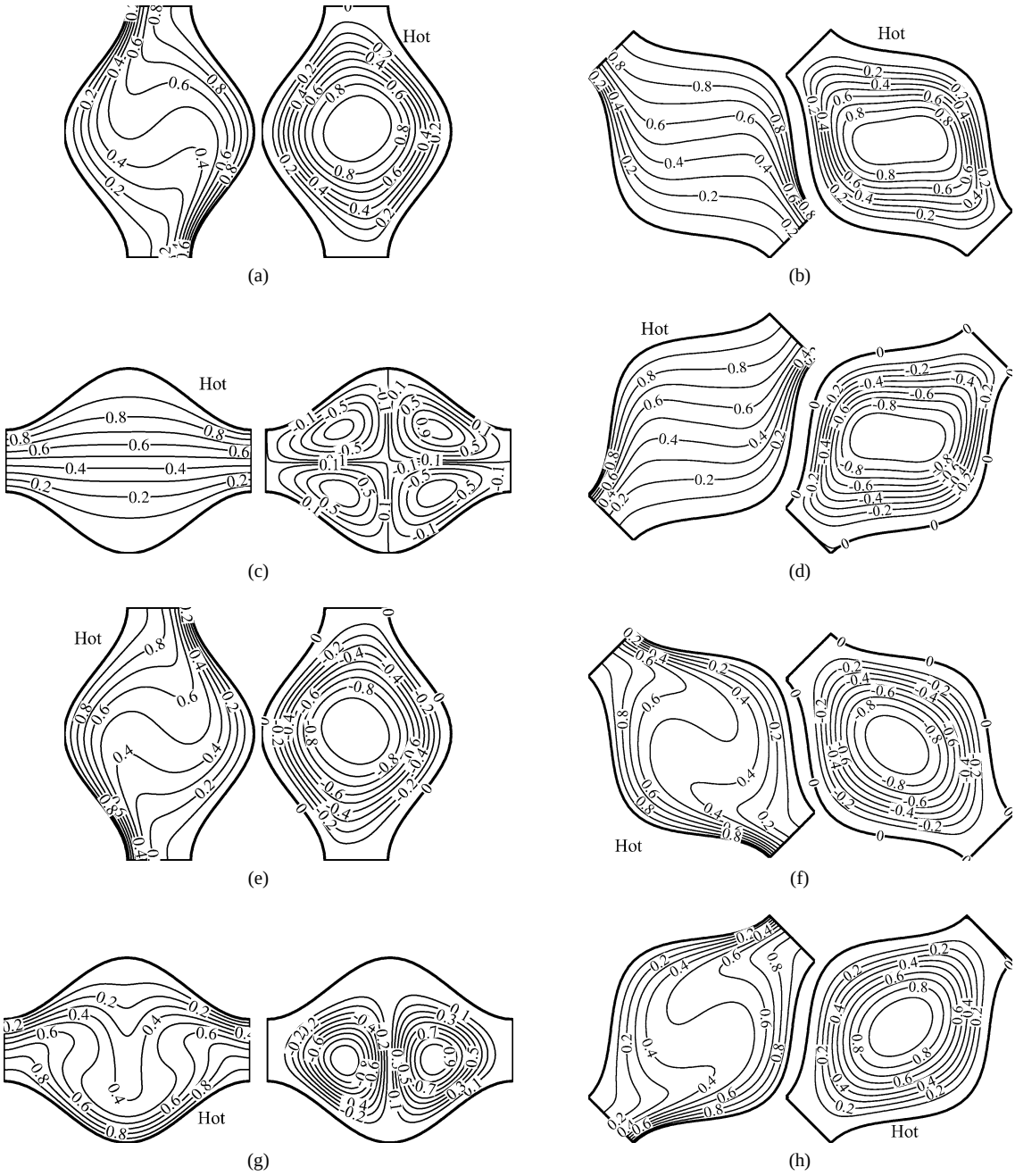

Fig. 3. Flow and thermal fields at different angles of inclination: (a) $\theta = 0°$, $\psi_{max} = 0.01221$; (b) $\theta = 45°$, $\psi_{max} = 0.00631$; (c) $\theta = 90°$, $\psi_{max} = 0.000468$; (d) $\theta = 135°$, $\psi_{max} = 0.00631$; (e) $\theta = 180°$, $\psi_{max} = 0.01221$; (f) $\theta = 225°$, $\psi_{max} = 0.016291$; (g) $\theta = 270°$, $\psi_{max} = 0.008193$; (h) $\theta = 315°$, $\psi_{max} = 0.016281$.

mixes with the fluid that moves downwards along the cold wall. This makes the circulation inside the cavity. Convection current is sufficiently strong at $Ra = 10^5$, which causes the convective distortion of isotherms. The lower portion of the hot wall and the upper portion of cold the wall are identified as the strong concentrators of isotherms. Two factors are simultaneously responsible for the high concentration of the isotherms at the above-mentioned position. The first factor is the fluid-jet (right to left near top adiabatic wall and left to right near bottom adiabatic wall) turned by the adiabatic walls and directed towards the opposite wall due to the high convection current. The second factor is the curvature of the wall. Concentration of isotherms causes high temperature gradient. Heat transfer rate is essentially high at these two spots. At $\theta = 45°$ (Fig. 3(b)), the core of the streamlines is elongated at the horizontal direction. Two comparatively weaker spots of high temperature gradient are observed at the lower part of the hot wall and upper part of the cold wall. Fluid is almost motionless at $\theta = 90°$ showing no swirls in the isotherms. Isotherms nearly follow the geometry of the

wavy walls. Fluid is very much stable at this angular position of the cavity ($\psi_{\max} = 0.000468$). It should be noted that the strength of the flow, at $\theta = 90°$, is approximately 34 times weaker than the flow at $\theta = 225°$ and 315°. Motion of the fluid is reversed at $\theta = 135°$ as indicated by the negative values of streamfunction. Core of the streamlines is elongated horizontally similar to $\theta = 45°$ but opposite in shape. Flow and thermal field at $\theta = 180°$ is similar (but opposite in direction) to $\theta = 0°$. Two counter rotating cells are observed at $\theta = 270°$. Fluid is at the most unstable condition at this angular position. Isothermal lines show swirling pattern but symmetrical about the mid-plan of the cavity. Flow and thermal field at $\theta = 315°$ is similar (but opposite in direction) to $\theta = 225°$.

3.2. Local heat transfer

Heat transfer rate is presented in terms of local and average Nusselt number. Local Nusselt number (Nu_L) is calculated from the following equation

$$Nu_L = \frac{W}{k} h_L = \frac{W}{k} \left\{ \frac{k}{\Delta T} \left(\frac{\mathrm{d}T}{\mathrm{d}n} \right)_w \right\} = \left(\frac{\mathrm{d}\Theta}{\mathrm{d}\hat{n}} \right)_w \tag{8}$$

In the above equation, h_L is the local convective heat transfer coefficient. The term '$(\partial T/\partial n)_w$' represents the temperature gradient normal to the wall where n is the normal distance and $\hat{n}$ is the dimensionless normal distance. Distribution of local Nusselt number along the hot wall is presented in Fig. 4 and Fig. 5 for two different Rayleigh numbers, $Ra = 10^3$ and 10^5, for a constant surface waviness ($\lambda = 0.25$) and aspect ratio ($A = 2.0$). At $Ra = 10^3$, convection is less dominant, isotherms follow mainly the surface geometry showing minimum temperature gradient at the middle of the cavity where cross-sectional area is maximum. Whatever the orientation (θ) of the cavity, local Nusselt number distribution shows a wavy patterns as shown in Fig. 4; minimum heat transfer occurs at the middle of the cavity due to the maximum cross-sectional area and maximum at the ends. Heat transfer rate is almost same in magnitude at the middle of the cavity for all values of θ. For $Y < 0.5$, heat transfer rate is slightly lower in magnitude for higher value of θ and this scenario is reversed for $Y > 0.5$. Convection dominates and boundary layer appears at $Ra = 10^5$. Local Nusselt number falls gradually along the wall at $\theta = 0°$ (see Fig. 5). For a range $0.5 \leqslant Y \leqslant 0.75$, Nusselt number does not vary with Y. Isotherms starts swirling due to high convective current at this Rayleigh number for $\theta = 0°$. Isothermal line close to the hot wall maintains a constant distance for this range ($0.5 \leqslant Y \leqslant 0.75$) showing constant temperature gradient as well as Nusselt number. Similar pattern is observed at $\theta = 180°$. For $\theta = 45°$, Nusselt number falls gradually up to $Y = 0.5$. After $Y = 0.5$, variation of Nusselt number is almost independent of Y up to the other end of the cavity. Same nature is observed in the Nusselt number distribution for $\theta = 135°$. At the cavity orientation $\theta = 90°$, fluid is almost motionless

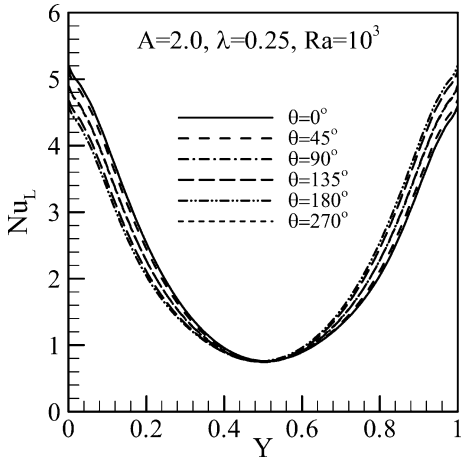

Fig. 4. Variation of local Nusselt number with Y at $Ra = 10^3$.

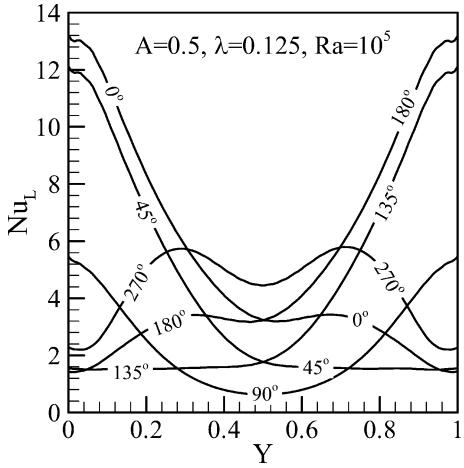

Fig. 5. Variation of local Nusselt number with Y at $Ra = 10^5$.

inside the cavity. At this angular position, local Nusselt number distribution at $Ra = 10^5$ shows similar pattern as $Ra = 10^3$. At $\theta = 270°$, bicellular flow appears and local Nusselt number shows periodic distribution along the hot wall.

3.3. Average heat transfer

Average Nusselt number is calculated by integrating local Nusselt number distribution using the following equation

$$Nu_{\mathrm{av}} = \frac{1}{S} \int_0^S Nu_L \, \mathrm{d}s \tag{9}$$

where s is the distance along the wavy wall and S is the total length of the wavy wall which can be calculated using the following expression

$$S = \int_0^A \sqrt{1 + \left(\frac{\mathrm{d}X}{\mathrm{d}Y} \right)} \, \mathrm{d}Y = \frac{A^2 + 2\lambda^2 \pi^2}{A} \tag{10}$$

Fig. 6 shows the distribution of average Nusselt number as

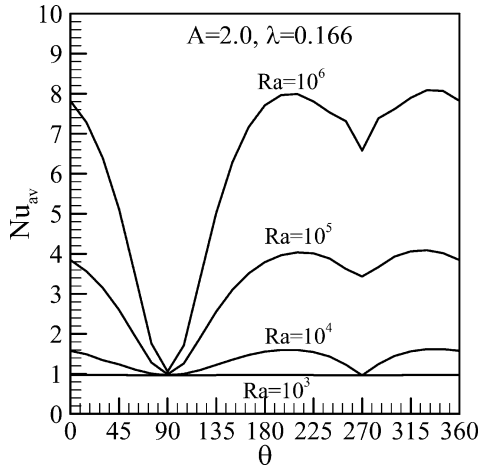

Fig. 6. Variation of average Nusselt number with angle of inclination.

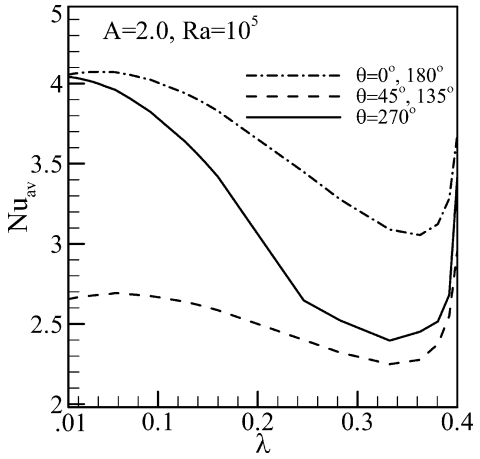

Fig. 7. Variation of average Nusselt number with surface waviness.

a function of angle of inclination (θ) at different Rayleigh numbers for $\lambda = 0.166$ and $A = 2.0$. For a particular angular position θ, average Nusselt number increases with the increase of Rayleigh number except $\theta = 90°$. For $Ra > 10^3$, average Nusselt number gradually decreases with the increase of θ up to $\theta = 90°$ where $Nu_{av} = 1.0$ for all values of Rayleigh numbers. Further increase of θ increase the average Nusselt number and shows a maximum at $\theta \approx 200°$. Additional increase of θ decreases the average Nusselt number up to $\theta = 270°$. After $\theta = 270°$, average Nusselt number again increases with θ and shows the second maximum at $\theta \approx 335°$ and again decreases.

3.4. Effect of surface waviness

Fig. 7 shows the distribution of average Nusselt number as a function of surface waviness (λ) for $A = 2.0$ and $Ra = 10^5$ for some selected values of θ. Three distinct zones are identified depending on the pattern of average Nusselt number variation with λ. Very lower values of surface waviness ($\lambda \leqslant 0.05$) does not play any effective role on average heat transfer. Heat transfer is invariant with surface waviness below $\lambda \approx 0.05$. In the middle range of surface waviness ($0.05 \leqslant \lambda < 0.325$), heat transfer gradually falls with the increase of surface waviness approximately up to $\lambda \approx 0.35$. Further increase of λ increases average Nusselt number. At high waviness (i.e., $\lambda > 0.35$), interwall spacing closer to the top end becomes small causing no convective distortion of isotherms. Isotherms remain concentrated at the wall and heat transfer is entirely dominated by conduction showing high rate of heat transfer at this portion. Fig. 8 will give a clear idea about the surprising rise of average Nusselt number at higher λ. For a particular position $\theta = 0°$, local Nusselt number is plotted as a function of Y in Fig. 8 for three different but comparatively higher values of λ (= 0.25, 0.32, 0.4). For $0 \leqslant Y \leqslant 0.9$, magnitude of Nu_L is more or less same. A drastic rise of Nusselt number occurs after $Y \approx 0.9$ for $\lambda = 0.4$. The magnitude of Nu_L is comparatively higher than $\lambda = 0.25$ and 0.32 for this range

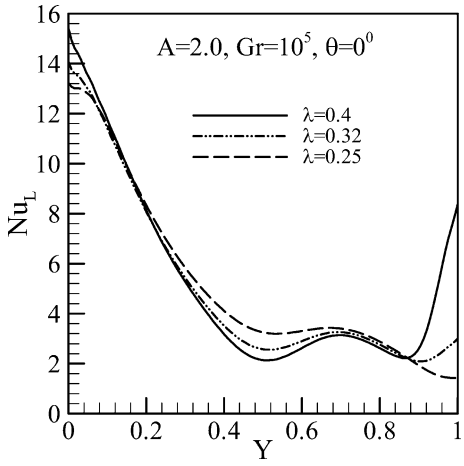

Fig. 8. Local Nusselt number variation with Y at different λ.

($0.9 \leqslant Y \leqslant 1.0$). So, when integrated, distribution of Nu_L at $\lambda = 0.4$ gives higher Nu_{av} than $\lambda = 0.32$ and 0.25. This type of behavior is restricted to higher values of λ.

3.5. Effect of aspect ratio

Fig. 9 shows the variation of average Nusselt number as a function of Rayleigh number for three different aspect ratio $A = 1.0$, 1.5, 2.0 at a constant surface waviness ($\lambda = 0.25$) and angular position ($\theta = 0°$). Based on the Rayleigh number two distinct zones can be identified from the figure. For $Ra \leqslant 10^3$, average Nusselt number is constant (≈ 1.0) and independent of Rayleigh number whatever the value of aspect ratio. This is actually the conduction regime. For $Ra \geqslant 10^3$, Nusselt number increases with Rayleigh number. For a particular Rayleigh number, lower aspect ratio shows the higher heat transfer rate. Comparatively smaller Interwall spacing for lower aspect ratio set the isotherms more close to the wall, which causes a high temperature gradient. When integrated for calculating total heat transfer, cavity with lower aspect ratio shows higher Nu_{av} distribution.

4. Entropy generation

The dimensionless form of entropy generation rate (N_S), given in Eq. (5), consists of two parts. The first part (first square bracketed term at the right-hand side of Eq. (5)) is the irreversibility due to finite temperature gradient and generally termed as heat transfer irreversibility (HTI). The second part is the contribution of fluid friction irreversibility (FFI) to entropy generation, which can be calculated from the second square bracketed term. The overall entropy generation, for a particular problem, is an internal competition between HTI and FFI. Usually, free convection problems, at low and moderate Rayleigh numbers, are dominated by the heat transfer irreversibility (discussed later in details). Entropy generation number (N_S) is good for generating entropy generation profiles or maps but fails to give any idea whether fluid friction or heat transfer dominates. Bejan [20] proposed irreversibility distribution ratio (Φ), which is the ratio between FFI and HTI. As an alternative irreversibility distribution parameter, Paoletti et al. [25] defined Bejan number (*Be*) which is the ratio of HTI to the total entropy generation. Mathematically Bejan number becomes

$$Be = \frac{\text{HTI}}{\text{HTI} + \text{FFI}} = \frac{1}{1 + \Phi} \tag{11}$$

Bejan number ranges from 0 to 1. Accordingly, $Be = 1$ is the limit at which the heat transfer irreversibility dominates, $Be = 0$ is the opposite limit at which the irreversibility is dominated by fluid friction effects, and $Be = 1/2$ is the case in which the heat transfer and fluid friction entropy generation rates are equal.

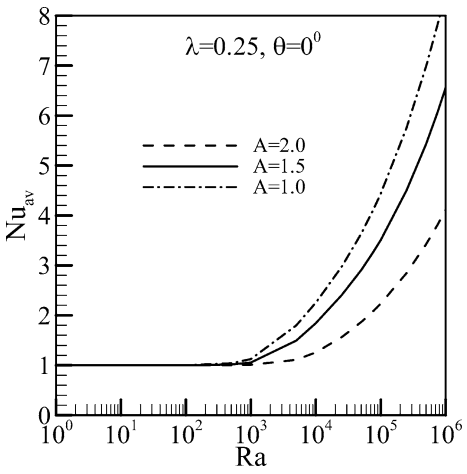

Fig. 9. Variation of average Nusselt number with aspect ratio.

For a constant aspect ratio (= 2.0) and surface waviness (= 0.125), Fig. 10 shows the contours of Bejan number for $Ra = 10$–10^6 and $\theta = 0°$. For each case, maximum and minimum values of Bejan number ($Be_{\max}$ and $Be_{\min}$) are indicated at the figure titles. Difference between the magnitudes of two consecutive Bejan contours is equal to $(Be_{\max} - Be_{\min})/10$. At low Rayleigh numbers, fluid is almost mo-

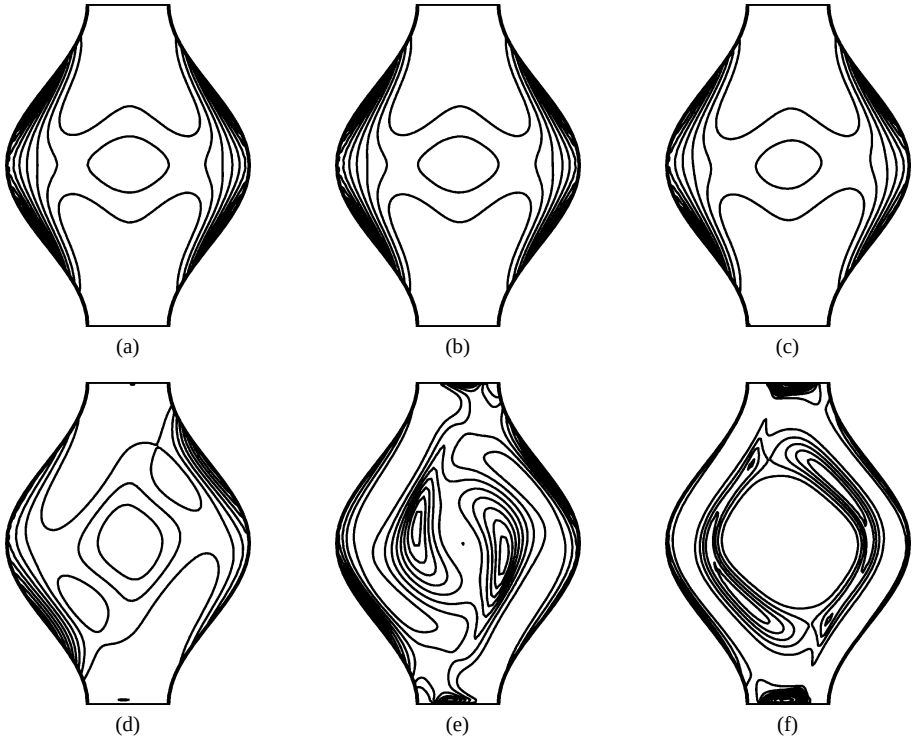

Fig. 10. Contours of Bejan number at different Rayleigh number and $\theta = 0°$: (a) $Ra = 10^1$, $Be_{\max} = 1$, $Be_{\min} = 0.99$; (b) $Ra = 10^2$, $Be_{\max} = 1$, $Be_{\min} = 0.98$; (c) $Ra = 10^3$, $Be_{\max} = 1$, $Be_{\min} = 0.89$; (d) $Ra = 10^4$, $Be_{\max} = 1$, $Be_{\min} = 0.61$; (e) $Ra = 10^5$, $Be_{\max} = 1$, $Be_{\min} = 0.51$; (f) $Ra = 10^6$, $Be_{\max} = 1$, $Be_{\min} = 0.16$.

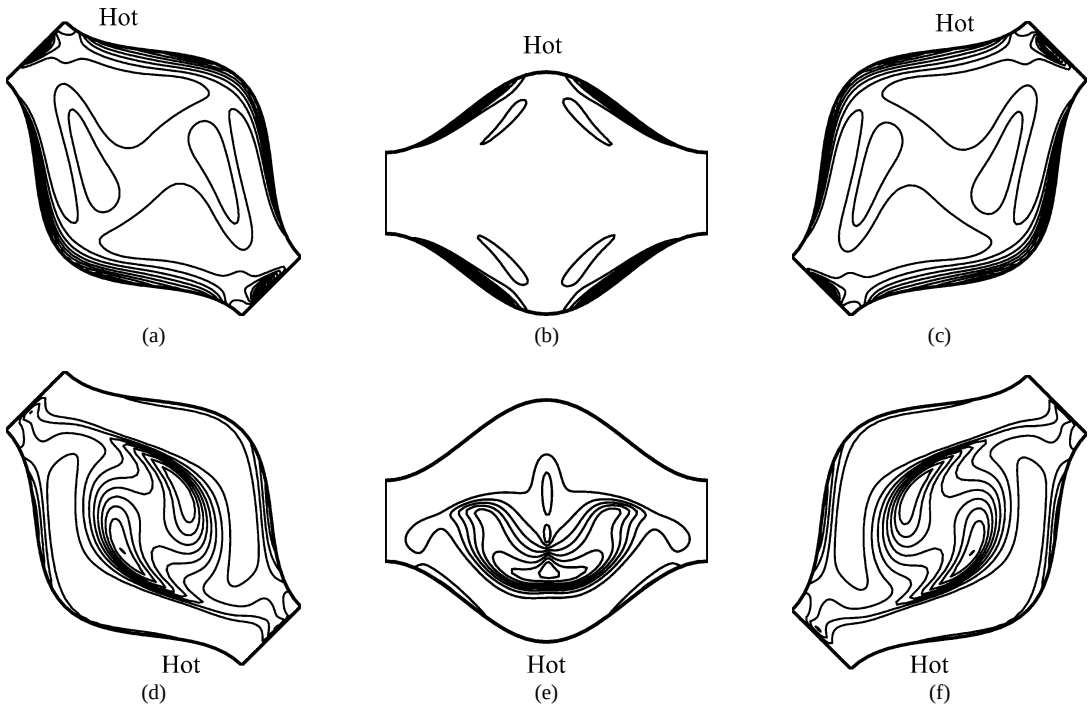

Fig. 11. Contours of Bejan number at different angles of inclination and $Ra = 10^5$. (a) $\theta = 45°$, $Be_{max} = 1$, $Be_{min} = 0.82$; (b) $\theta = 90°$, $Be_{max} = 1$, $Be_{min} = 0.97$; (c) $\theta = 135°$, $Be_{max} = 1$, $Be_{min} = 0.82$; (d) $\theta = 255°$, $Be_{max} = 1$, $Be_{min} = 0.19$; (e) $\theta = 270°$, $Be_{max} = 1$, $Be_{min} = 0.21$; (f) $\theta = 315°$, $Be_{max} = 1$, $Be_{min} = 0.19$.

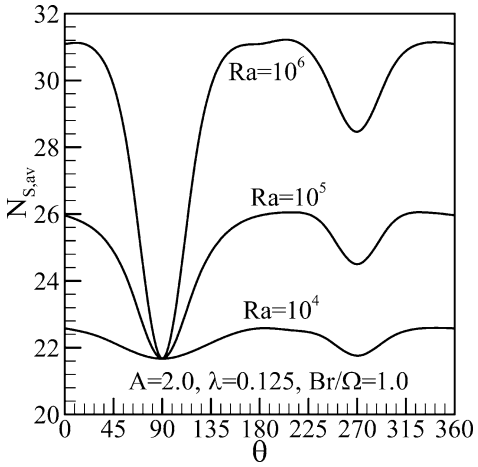

Fig. 12. Variation of average entropy generation number with angle of inclination.

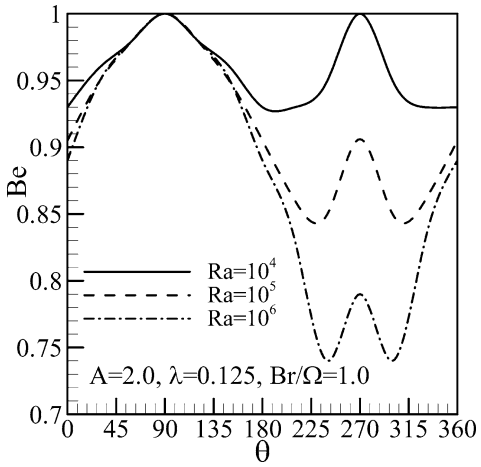

Fig. 13. Variation of Bejan number with angle of inclination.

tionless in the cavity. Irreversibility is entirely dominated by heat transfer. Bejan contour shows symmetric distribution at $Ra = 10$, 10^2 and 10^3. Near wall concentration of Bejan contours indicates the region of high irreversibility. Convection current becomes stronger at higher Rayleigh numbers resulting distortion of isotherms. Near the core region of the cavity, nonzero $\partial\Theta/\partial Y$ starts dominating. With the increase of Rayleigh number, zone of irreversibility at the core region becomes narrow. For $Ra = 10^5$, Bejan contours are presented in Fig. 11 for six different orientations and constant aspect ratio and waviness. At $\theta = 45°$ and 135°, the region of irreversibility is elongated along the wavy walls compared to its vertical position (Fig. 10(d)). At $\theta = 90°$, small regions of wavy walls are identified as concentrator of irreversibility. It should be noted that the fluid is almost motionless at this position of the cavity. At $\theta = 225°$ and 315°, due to the convective distortion of isotherms, heat transfer irreversibility occurs near wavy walls as well as the core region of the cavity. Due to the appearance of bicellular flow and swirling nature of isotherms at $\theta = 270°$, a complicated Bejan contour distribution is observed.

A volume averaged entropy generation rate ($N_{S,\mathrm{av}}$) is calculated using the following equation

$$N_{S,\mathrm{av}} = \frac{1}{\forall}\int_{\forall} N_S \,\mathrm{d}\forall \tag{12}$$

where $\forall$ is the volume of the cavity. Fig. 12 shows the variation of $N_{S,\mathrm{av}}$ with θ at $Ra = 10^4$, 10^5 and 10^6 keeping surface waviness ($= 0.125$), aspect ratio ($= 2.0$) and group parameter ($= 1.0$) constant. Distribution pattern of $N_{S,\mathrm{av}}$ with θ is very much similar to $Nu_{\mathrm{av}}-\theta$ distribution as shown in Fig. 6. For each Rayleigh number, rate of average entropy generation falls with increasing θ showing its minimum value at $\theta = 90°$. At this angular position, entropy generation is same in magnitude of all Rayleigh numbers. $Nu_{S,\mathrm{av}}-\theta$ distribution is symmetric about for $0° \leqslant \theta \leqslant 180°$. The second symmetrical distribution of $Nu_{S,\mathrm{av}}$ with θ is observed for $180° \leqslant \theta \leqslant 360°$. Based on the average values of FFI and HTI, Bejan number is calculated and plotted in Fig. 13 for the same flow and geometric parameters as shown in Fig. 12.

5. Conclusions

Heat transfer characteristics with flow structure are studied numerically in this paper for a cavity with differentially heated wavy walls and adiabatic flat walls. Effect of aspect ratio, surface waviness on heat transfer is tested at different Rayleigh numbers and angle of inclination. For a particular aspect ratio, heat transfer is constant and independent of Rayleigh number at conduction regime determined by certain range of Ra ($Ra \leqslant 10^3$). Above this range, heat transfer increases with the increase of Rayleigh number. Lower is the surface waviness, higher is the heat transfer for a particular angular position. Average heat transfer shows a well-shaped variation with the angle of inclination of the cavity. Two distinct peaks for average Nusselt number is found at $\theta \approx 200°$ and $\theta \approx 335°$, respectively. Heat transfer is minimum at $\theta = 90°$ for all Rayleigh numbers. For a particular aspect ratio and angular position, average Nusselt number gradually falls with surface waviness (λ) except the higher values of λ after which Nu_{av} starts to increase. Volume averaged entropy generation rate shows the similar distribution pattern with θ as average Nusselt number.

References

[1] L. Adjlout, O. Imine, A. Azzi, M. Belkadi, Laminar natural convection in an inclined cavity with a wavy wall, Internat. J. Heat Mass Transfer 45 (2002) 2141–2152.

[2] S. Mahmud, P.K. Das, N. Hyder, A.K.M. Islam, Free convection in an enclosure with vertical wavy walls, Internat. J. Thermal Sci. 41 (2002) 440–446.

[3] A. Hadjadj, M.E. Kyal, Effect of two sinusoidal protuberances on natural convection in a vertical annulus, Numer. Heat Transfer Part A 36 (1999) 273–289.

[4] B.V.R. Kumar, A study of free convection induced by a vertical wavy surface with heat flux in a porous enclosure, Numer. Heat Transfer Part A 37 (2000) 493–510.

[5] L.S. Yao, Natural convection along a vertical wavy surface, J. Heat Transfer 105 (1983) 465–468.

[6] C. Saidi, F. Legay, B. Pruent, Laminar flow past a sinusoidal cavity, Internat. J. Heat Mass Transfer 30 (1987) 649–660.

[7] Y. Asako, M. Faghri, Finite volume solution for laminar flow and heat transfer in a corrugated duct, J. Heat Transfer 109 (1987) 627–634.

[8] S. Mahmud, A.K.M. Islam, P.K. Das, Numerical prediction of fluid flow and heat transfer in a wavy pipe, Internat. J. Thermal Fluid Sci. 10 (2001) 133–138.

[9] J.L. Lage, A. Bejan, Convection from a periodically stretching plane wall, J. Heat Transfer 112 (1990) 92–99.

[10] M.A. Hossain, D.A.S. Rees, Combined heat and mass transfer in natural convection flow from a vertical wavy surface, Acta Mech. 136 (1999) 133–141.

[11] S.G. Moulic, L.S. Yao, Natural convection along a wavy surface with uniform heat flux, J. Heat Transfer 111 (1989) 1106–1108.

[12] D.A.S. Rees, I. Pop, Free convection induced by a vertical wavy surface with uniform heat transfer flux in a porous medium, J. Heat Transfer 117 (1995) 545–550.

[13] F.J. Hamady, J.R. Lloyd, H.Q. Yang, K.T. Yang, Study of local natural convection heat transfer in an inclined enclosure, Internat. J. Heat Mass Transfer 32 (1989) 1697–1708.

[14] H. Ozoe, H. Sayma, S.W. Churchill, Natural convection in an inclined rectangular channel at various aspect ratios and angles—Experimental measurements, Internat. J. Heat Mass Transfer 18 (1975) 1425–1431.

[15] S.M. Elsherbiny, Free convection in inclined air layers heated from above, Internat. J. Heat Mass Transfer 39 (1996) 3925–3930.

[16] L.G. Sundstrom, S. Kimura, On laminar free convection in inclined rectangular enclosures, J. Fluid Mech. 313 (1996) 343–366.

[17] O. Aydin, A. Unal, T. Ayhan, A numerical study on buoyancy-driven flow in an inclined square enclosure heated and cooled on adjacent walls, Numer. Heat Transfer Part A 36 (1999) 585–899.

[18] A. Bejan, Entropy Generation Minimization, CRC Press, New York, 1996.

[19] A.C. Baytas, Entropy generation for natural convection in an inclined porous cavity, Internat. J. Heat Mass Transfer 43 (2000) 2089–2099.

[20] A. Bejan, A study of entropy generation in fundamental convective heat transfer, J. Heat Transfer 101 (1979) 718–725.

[21] S. Mahmud, R.A. Fraser, Second law analysis in fundamental convective heat transfer problems, Internat. J. Thermal Sci., submitted for publication.

[22] M. Hortmann, M. Peric, G. Scheuerer, Finite volume multigrid prediction of laminar natural convection: Benchmark solutions, Internat. J. Numer. Methods Fluids 11 (1990) 189–207.

[23] J. Ferziger, M. Peric, Computational Methods for Fluid Dynamics, Springer, Berlin, 1996.

[24] N.C. Markatos, K.A. Pericleous, Laminar and turbulent natural convection in an enclosed cavity, Internat. J. Heat Mass Transfer 27 (1984) 755–772.

[25] S. Paoletti, F. Rispoli, E. Sciubba, Calculation of exergetic losses in compact heat exchanger passages, ASME AES 10 (1989) 21–29.